

pubs.acs.org/ac Article

# Nanopore Analysis as a Tool for Studying Rapid Holliday Junction Dynamics and Analyte Binding

Madhav L. Ghimire, Dalton R. Gibbs, Roaa Mahmoud, Soma Dhakal, and Joseph E. Reiner\*



Cite This: Anal. Chem. 2022, 94, 10027-10034



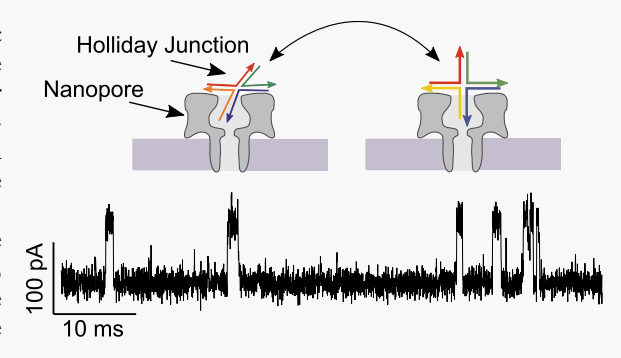
ACCESS I

Metrics & More

Article Recommendations

Supporting Information

ABSTRACT: Holliday junctions (HJs) are an important class of nucleic acid structure utilized in DNA break repair processes. As such, these structures have great importance as therapeutic targets and for understanding the onset and development of various diseases. Single-molecule fluorescence resonance energy transfer (smFRET) has been used to study HJ structure-fluctuation kinetics, but given the rapid time scales associated with these kinetics (approximately sub-milliseconds) and the limited bandwidth of smFRET, these studies typically require one to slow down the structure fluctuations using divalent ions (e.g., Mg<sup>2+</sup>). This modification limits the ability to understand and model the underlying kinetics associated with HJ fluctuations. We address this here by utilizing nanopore sensing in a gating configuration to monitor DNA



structure fluctuations without divalent ions. A nanopore analysis shows that HJ fluctuations occur on the order of 0.1–10 ms and that the HJ remains locked in a single conformation with short-lived transitions to a second conformation. It is not clear what role the nanopore plays in affecting these kinetics, but the time scales observed indicate that HJs are capable of undergoing rapid transitions that are not detectable with lower bandwidth measurement techniques. In addition to monitoring rapid HJ fluctuations, we also report on the use of nanopore sensing to develop a highly selective sensor capable of clear and rapid detection of short oligo DNA strands that bind to various HJ targets.

#### ■ INTRODUCTION

Holliday junctions (HJs) are critical intermediates of a DNA repair pathway and are formed in cells during the repair of double-strand DNA breaks. DNA is highly susceptible to damage caused by external factors such as radiation and reactive oxygen species (ROSs). Such breaks are repaired in a process called homologous recombination (HR), in which a second copy of the genome is used as a template, leading to the formation of four-way structures commonly known as HJs.<sup>2-</sup> For HR to be successful, the junction must be properly formed and eventually resolved back into two separate doublestranded DNA (dsDNA) molecules. Given the important role HJs play in DNA repair, it is easy to see why they are a promising target for therapeutics.<sup>6-8</sup> Furthermore, besides their biological roles and potential therapeutic applications, HJs have been exploited in several other nonbiological applications such as nucleic acid sensing and the design of smart DNA devices. 9-11 Therefore, to fully realize the potential of HJs in these applications, we need to better understand the molecular properties of the junctions.

Isolated HJs have been characterized by single-molecule techniques such as single-molecule fluorescence resonance energy transfer (smFRET) and time-resolved FRET. These techniques have shown that HJs undergo isomerization between two main isomers, namely, *iso-I* and *iso-II*, via a transient plus-like (*open*) conformation. While some key

insights on the molecular behavior of HJs have been identified (i.e., the dynamics are heavily affected by microenvironments such as ionic strength and the core sequence of the junction), there is a need for a technology that is sensitive to these subtle conformational changes and capable of identifying these states at high frequencies (>1 kHz). While smFRET is heavily used to study HJs, <sup>14,16</sup> the technique requires slowing down the dynamics of HJs to enable sufficient capture of different FRET states. <sup>17</sup> In this manuscript, we utilize a nanopore platform to investigate the kinetic and dynamic behavior of the HJs at high frequency and analyte binding with the pore-bound HJ molecules.

Nanopore sensors have been widely used to study various aspects of DNA properties at the molecular level. These include DNA unzipping kinetics, <sup>18</sup> DNA and RNA sequencing, <sup>19,20</sup> analysis of various DNA secondary structures, <sup>21–23</sup> real-time monitoring of protonation/deprotonation of nucleotides, <sup>21,24</sup> nucleotide substitutions, <sup>25,26</sup> and many more. <sup>27–31</sup>

Received: January 21, 2022 Accepted: June 21, 2022 Published: July 5, 2022





However, there is a lack of nanopore analysis of dsDNA and supramolecular structures involving dsDNA. This is mostly because the workhorse of the biological nanopore sensing community,  $\alpha$ -hemolysin ( $\alpha$ HL), is too narrow to permit the transit of dsDNA.<sup>20</sup> This has been addressed to some degree with the study of other nanopore sensors both biological (i.e., doubly mutated Fragaceatoxin C (ReFraC))<sup>32</sup> and solidstate.<sup>33</sup> Of particular interest is the work done with the outer membrane protein G  $(OmpG)^{34}$  and aptamer-modified  $\alpha HL$ pores for thrombin detection.<sup>35</sup> In these cases, current signatures were modified by molecular fluctuations occurring outside the pore volume. This sensing configuration has been referred to as a gating sensor, 30 and it is advantageous because it enables the detection of molecules larger than the pore itself. This configuration addresses a common criticism of nanopore analysis, where the nanoconfined environment of the pore modifies the degrees of freedom or entropic component of the molecular free energy landscape. Here, we use nanopores operating in the gating sensor mode to study secondary structure-fluctuation kinetics of HJs external to the pore.

To demonstrate the feasibility of using  $\alpha$ HL as a viable nanopore for studying HJs, we establish that the dsDNA structures can be efficiently captured in the cis-side vestibule of the pore for extended periods (>5 s). These capture events yield well-defined fluctuations that are associated with transitions between the different conformations of HJs. smFRET studies of HJ dynamics usually require the addition of divalent ions to slow down the HJ fluctuations so they are observable at typical wide-field FRET sampling rates. 17,36 Given the bandwidth of the nanopore detection system (10 kHz), we are able to monitor HJ fluctuations for extended periods (tens of seconds and longer) at a much higher temporal resolution than in smFRET measurements. This increased bandwidth enables one to detect HJ dynamics without divalent ions, and we find HJ fluctuations occurring on the order of 0.1-10 ms.

In addition to monitoring HJ dynamics, we also demonstrate that the pore-bound HJ can be used as a single-molecule sensor for short-strand DNA oligos. This requires modification to the HJ with a single-stranded overhang extending from one arm of the HJ molecule. We show that the presence of this arm does not interfere significantly with the HJ isomer fluctuations. This overhang serves as a template onto which a DNA target can bind, and upon binding we find that the rapid HJ fluctuations cease or change in a significant manner that yields a clear and easily detectable modification of the current. Ligand binding with HJs represents an important class of problems relevant for the development of therapeutics. Therefore, our work shows that the nanopore could serve as an excellent sensor for label-free HJ adsorption or binding studies.

This work serves as a demonstration of the benefits that nanopore sensing can provide when operated in the gating sensor configuration. Molecules larger than the pore have received less attention in the nanopore community given the lack of sizing information that can be extracted from molecular fluctuations outside the pore. Nevertheless, these fluctuations can be observed over extended periods at time scales inaccessible to other single-molecule methods (i.e., smFRET). Additionally, the molecular fluctuations outside the pore serve as an ideal target for single-molecule sensing. Both applications reported here suggest a powerful measurement technique that can elucidate previously inaccessible information about DNA secondary structures.

#### EXPERIMENTAL SECTION

**Materials.** All chemicals for nanopore experiments, unless otherwise specified, were purchased and used as received from Sigma-Aldrich Corp. 1,2-Diphytanoyl-sn-glycero-3 phosphocholine (DPhy:PC) was purchased from Avanti Polar Lipids. Teflon sheets were purchased from Goodfellow Corporation, and laser-drilled 50  $\mu$ m holes were formed in the sheets at Potomac Photonics. Borosilicate glass capillaries (OD = 1.0 mm, ID = 0.5 mm, 0.78 mm) were purchased from Sutter Instruments. n-Pentane was purchased from Fisher Scientific.  $\alpha$ -Toxin from Staphylococcus aureus was purchased from IBT Bioservices.

For smFRET experiments, tris(hydroxymethyl)-aminomethane(tris), ethylenediaminetetraacetic acid disodium salt (EDTA), KCl, glycerol, biotinylated bovine serum albumin (bBSA), 6-hydroxy-2,5,7,8-tetramethylchroman-2-carboxylic acid (Trolox), and Protocatechuate 3,4-dioxygenase (PCD) were purchased from Fisher Scientific. PCD was suspended in a pH 8.0 PCD buffer (100 mM Tris-HCl, 50 mM KCl, 1 mM EDTA, 50% glycerol), sterile-filtered using a 0.2  $\mu$ m filter, and stored at  $-20~^{\circ}$ C. Magnesium chloride hexahydrate was purchased from Arcos Organics. Sodium chloride, streptavidin, protocatechuic acid (PCA), 30% ammonia/water, and hydrogen peroxide were purchased from VWR.

DNA Constructs. All DNA strands were purchased as oligomers from Integrated DNA Technologies (IDT) and stored at -20 °C. All HJ DNA constructs (Supporting Information, Table S1) were assembled with a thermal annealing protocol of the relevant oligomers in 1X TAE buffer (pH 7.4) (40 mM Tris, 20 mM acetic acid, and 1 mM EDTA) using a temperature ramp from 95 to 4 °C as previously described. <sup>17,21,41</sup> DNA construct structures are illustrated in Figure S1 of the Supporting Information.

KCl Imaging Buffer. KCl imaging buffer (1 M KCl, 50 mM MgCl<sub>2</sub>, 137 mM NaCl, 12 mM Na<sub>2</sub>HPO<sub>4</sub>, 2 mM PCA, 5 mM Trolox, and 50 nM PCD) contains as much KCl as is possible without significant background fluorescence saturating the image and a protocatechuic acid/protocatechuate-3,4-dioxygenase oxygen scavenging system to minimize photobleaching of fluorophores.<sup>17,42</sup>

Nanopore Sensing Setup and Methodology. Singlechannel recordings were performed using an  $\alpha$ HL nanopore in an unsupported lipid bilayer membrane composed of DPhy:PC lipid. This methodology has been described elsewhere. 43-45 Briefly, a 20  $\mu$ m thick Teflon partition with a single 50  $\mu$ m diameter hole was fixed onto a Teflon support and pretreated with  $1-2 \mu L$  of a 1 mg/mL DPhy:PC in pentane prepaint solution. After the pentane evaporated, the Teflon partition was immersed in a 3 M KCl, 1 mM Tris-EDTA electrolyte buffer at pH 7.4. We did not use 50 mM MgCl<sub>2</sub> in the nanopore buffer because divalent cations have been shown to cause spurious gating to the wild-type  $\alpha$ -hemolysin pore. This could give rise to random fluctuations that would complicate interpretations of the nanopore measurements. 46 Future studies will explore modifications to solution conditions to enable closer matching between the nanopore and imaging buffers. To form the membrane, a small volume of lipid solution (ca. 10 pL of 10 mg/mL DPhy:PC dissolved in hexadecane) was ejected from a micropipette capillary near the 50  $\mu$ m hole, and a glass ball was used to "paint" this lipid solution over the hole until a membrane formed. A single  $\alpha HL$ channel was inserted into the membrane with a tip-insertion

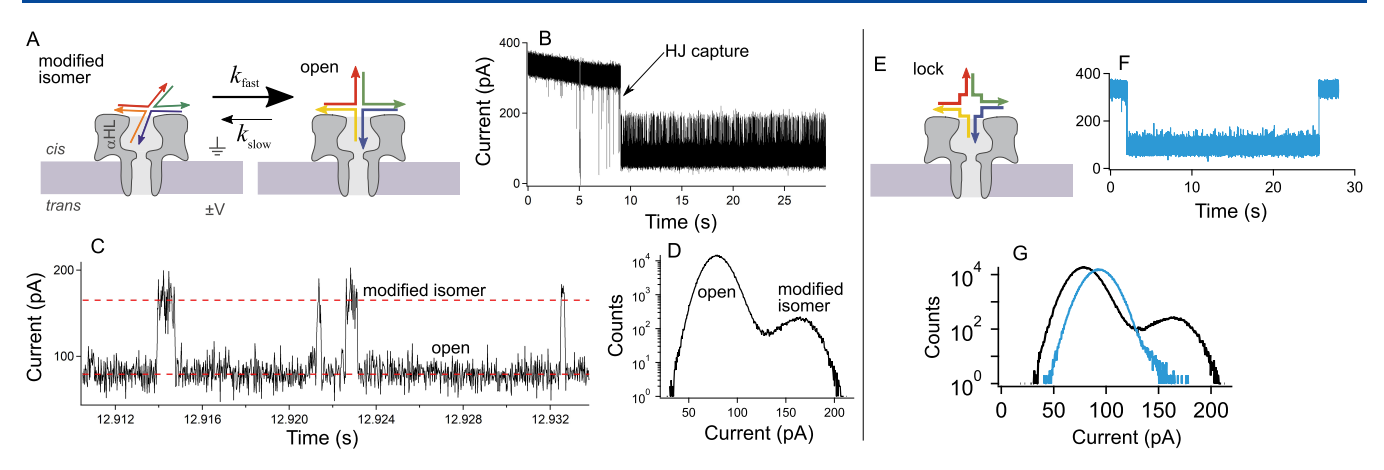


Figure 1. Schematic illustration of the nanopore approach and sample current traces that illustrate rapid Holliday junction fluctuations. (A) A cartoon schematic of the pore-bound junction as we envision the fluctuating molecule's configuration. (B) A typical current trace shows the capture of a single junction at  $t \approx 9$  s corresponding to a rapid downward transition in the current. (C) Enlarged view of the current trace and (D) the corresponding all-points histogram highlights the two-state fluctuations between the two HJ states (open and isomer). (E) A control experiment with a mismatched inner pairing (I-HJ-0) yields a "locked" conformation. (F) The typical current trace of the locked junction and (G) the corresponding histogram shows the absence of two-state fluctuations. Data shown here were collected in 3 M KCl at pH 7.4 under an applied +140 mV transmembrane potential.

technique described elsewhere.<sup>45</sup> The complete setup was placed in an electrically grounded Faraday cage enclosure to reduce any external RF noise.

A nanopore-based detection of HJ molecules was performed by positioning a borosilicate glass capillary formed with preset program No. 11 (HEAT = 350, FIL = 4, VEL = 30, DEL = 200, PUL = 0) from a P-2000 laser puller (Sutter Instruments) applied to a capillary with OD = 1.0 mm and ID = 0.5 mm. The capillary contained 5  $\mu$ L of 2.5  $\mu$ M HJ molecules, and it was positioned ca. 100  $\mu$ m away from the membrane with a motorized manipulator (MPC-325, Sutter Instruments). After a voltage was applied across the membrane (V = 140 mVunless stated otherwise), the analyte was ejected from the capillary by applying a continuous pressure of ca. 15 hPa with a Femtojet standalone pump (Eppendorf). The Femtojet pump was left on until a rapid, downward transition in the current indicated the capture of a single HJ molecule. If the current remains in the captured state for several seconds ( $t \approx 5$  s), then the pump is turned off and remains off for the remainder of the event. In the case of target analyte detection, a second capillary tip, which contains the target analyte at various concentrations, is positioned near the membrane, and a second Femtojet pump ejects the target analyte under continuous pressure (typically 15 hPa) onto the pore-bound HJ molecule.

FRET Setup and Methodology. Surface-functionalized flow cells were prepared as previously described.  $^{17,21,47}$  Prepared flow cells were incubated with 20 pM HJ in phosphate-buffered saline (PBS) buffer for  $\approx 45$  s before being flushed with KCl imaging buffer. The slide was left for 5 min to equilibrate, and movies were taken. Slides were then flushed with a KCl imaging buffer containing 400 nM DNA target and left to incubate for 30 min before the imaging was done. All imaging was done on a custom-built single-molecule total internal reflection fluorescence microscope. Fluorescence was recorded on an electron-multiplying charge-coupled device (EMCCD) camera with a time resolution of 50 ms.

**Data Analysis.** *Nanopore Data Analysis.* The Axopatch 200B amplifier (Molecular Devices) was used to amplify the current, and current data were collected in voltage-clamp mode at a sampling rate of 50 kHz with a low-pass Bessel filter of 10

kHz using a Digidata 1550B analog-to-digital converter (Molecular Devices). Data were recorded with pCLAMP 10.7 software (Molecular Devices) and analyzed with CLAMPFIT 10.7 and IGOR 6.37 (Wavemetrics) software. Current—Time traces, histograms, and transition time distributions were obtained using the IGOR software.

FRET Data Analysis. Movies from the single-molecule FRET experiments were transformed into trace files using IDL and MatLab scripts as described in previous publications. <sup>17,21</sup> Single-molecule intensity traces, once generated, were chosen for analysis based on the presence of both single-step photobleaching and both Cy3 and Cy5 signals. The histograms of the traces were generated using the first 5 s of observation time of each trace. Visible populations were fit using Gaussian fitting in Origin pro.

# ■ RESULTS AND DISCUSSION

Nanopore sensing enables the loading and capture of individual HJ molecules for extended observation times. Figure 1 illustrates the principle of operation and a typical current trace that results from the capture and confinement of a single HJ molecule in the *cis*-side vestibule of an  $\alpha$ HL pore (Figure 1A). Sequence information for all DNA constructs used herein can be found in Table S1 of the Supporting Information.

Under an applied transmembrane potential, a capillary microtip preloaded with HJ molecules (hereafter referred to as HJ-0 because these have no single-strand overhangs) is ejected near the vicinity of the pore (ca. 100  $\mu$ m away). After several seconds, the capture event yields a downward stepwise transition in the current. The current appears to be confined to a stable level with rapid upward transitions to a second, less stable state (Figure 1B,C). An all-points histogram of the current (Figure 1D) from the trapped HJ-0 molecule in Figure 1B clearly indicates two-level fluctuations between (79  $\pm$  1) and (160  $\pm$  1) pA.

To confirm that the two-state fluctuations result from structural transitions of the trapped HJ-0 molecule and not spurious current fluctuations, we performed a control measurement using an HJ molecule with a mismatched core (Figure S1). We refer to this molecule as I-HJ-0 or interrupted-HJ-0,

where the mismatched sequence at the core of the junction is likely to yield a molecule locked in an open or cross configuration as shown in Figure 1E. The capture of an I-HJ-0 molecule shows no evidence of the two-state fluctuations. Instead, we found that this I-HJ-0 molecule yields a single-state blockade (Figure 1F) that nearly overlaps with the deeper state found with the HJ-0 molecule (Figure 1G). This leads to two conclusions: First, the rapid transitions between the two states seen in Figure 1C most likely result from structural transitions between isomer and open configurations of the HJ-0 molecule, and second, the near overlap between the open state of the HJ-0 molecule and the single state of the I-HJ-0 molecule suggests that the lower state in Figure 1C most likely corresponds to the open-state configuration, while the upper state corresponds to a so-called modified isomer configuration similar to the iso-I or iso-II configurations reported with smFRET measurements.  $^{17,49,50}$ 

On the basis of this, we propose a fluctuation scheme (illustrated in Figure 1A) where the trapped molecule resides on the top of the  $\alpha$ HL pore and undergoes rapid fluctuations from stacked isomer to open configuration and slower transitions back to the stacked isomer state. This is distinct from the reported observations in smFRET, where the isomer states are longer-lived while the open state is short and rapid, but it is possible that the HJ confinement in the nanopore and the applied force from the transmembrane potential could modify the HJ's kinetics. Although further studies are needed to more clearly elucidate these interesting conformational states associated with each current level, it is beyond the scope of the present manuscript.

Regardless of the conformational details of the pore-bound HJ-0 molecules, it is clear that the  $\alpha$ HL pore is capable of capturing and identifying structural fluctuations with rapid kinetics in a label-free manner, and this suggests that a nanopore analysis of HJs can provide insight into kinetics that are inaccessible to other single-molecule techniques. We stress that these measurements are performed in the absence of divalent ions, which are usually required to slow down the HJ kinetics for smFRET measurements.  $^{17,49,50}$ 

Figure 2 shows the variability among fluctuation types for both HJ-0 and I-HJ-0 molecules. We report all-points histograms of the postcapture current for 17 different HJ-0 molecules. To eliminate event-to-event variability, we subtract the peak current level from each trace (most abundant current level) and normalize each histogram to a peak value of 1. This aligns each distribution (see Figure 2A) and shows that the HJ-0 molecules can yield clear, two-state fluctuations (referred to as Type 3) like those seen in Figure 1C. Other fluctuation types that show little (Type 2) or no (Type 1) evidence of two-state fluctuations are also observed. It is not clear why we see a variety of blockade types for the HJ-0 molecules, but this could be related to specific interations between DNA bases and the protein channel (note that the sequence of each arm of HJ-0 is different, which may lead to slightly different interactions with the pore and hence a distribution of blockade dynamics) or the orientation of the HJ-0 molecules as they enter the pore. In any event, for comparison, we show current histograms for 18 different I-HJ-0 molecules, and these yield no evidence of two-state fluctuations, which confirms that Type 3 fluctuations result from structural changes of the HJ-0 molecules. Sample traces of each event type are shown in Figure 2B.

To quantify the kinetics for Type 3 fluctuations, we performed a thresholding analysis on three different Type 3

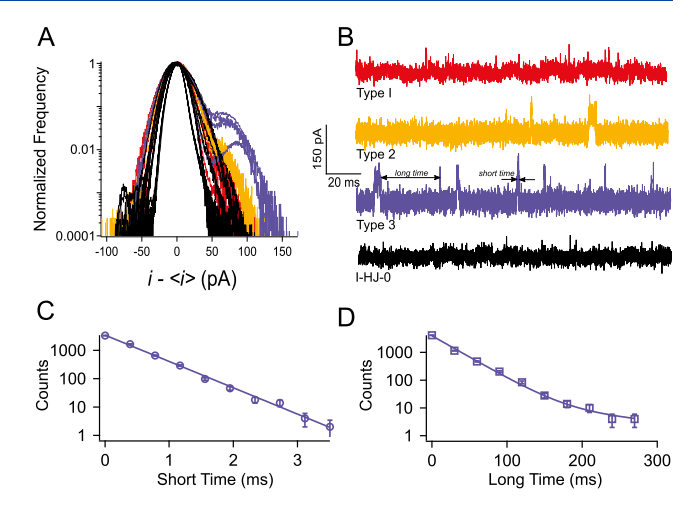


Figure 2. HJ-0 junctions yield distinct two-state current blockades. (A) The normalized and shifted blockade distributions for 17 different HJ-0 capture events (red, orange, and blue traces) show three distinct fluctuation types for HJ-0 molecules with a major peak and varying degrees of secondary peaks. For comparison, we also show current distributions for 18 different I-HJ-0 capture events (black traces). (B) Magnified sample current traces labeled as Types 1, 2, and 3 show a clear presence of the two-state fluctuations for the HJ-0 with no overhang. The color coding is consistent between parts (A) and (B). HJ-0 folding kinetics parametrized by the (C) short time and (D) long time distributions of the Type-3 kinetics are well-fit with single and double exponential distributions respectively (solid lines). Data shown here were collected in 3 M KCl at pH 7.4 under a +140 mV applied transmembrane potential. Residence time distributions were constructed from three different HJ-0 molecules.

events (3055 steps) to extract the short-time (time in the upper current state) and long-time (time in the lower current state) distributions shown in Figure 2C,D respectively. The short time distributions appear well-fit with single-exponential functions, and the long time events appear to be better described with a double-exponential distribution. The fitting results in a mean short time of  $t_{\rm short} = (0.47 \pm 0.1)$  ms and two mean long times of  $t_{\rm long,1} = (28 \pm 1)$  ms and  $t_{\rm long,2} = (160 \pm 95)$  ms. This corresponds to kinetic rates of  $k_{\rm fast} = (2100 \pm 450)$  s<sup>-1</sup> and  $k_{\rm slow,1} = (36 \pm 1)$  s<sup>-1</sup>,  $k_{\rm slow,2} = (6.3 \pm 3.7)$  s<sup>-1</sup>. With the exception of  $k_{\rm slow,2}$ , we find the kinetic rates that are larger than previously reported in smFRET studies  $^{17,49,50}$  but consistent with the fact that decreasing divalent ion concentrations will increase the rate of fluctuations.

In addition to using a nanopore analysis for studying HJ fluctuation kinetics, we also report on using trapped HJ molecules for sensing short DNA targets. HJ-based sensing requires an ssDNA overhang extending from one arm of the HJ molecule to serve as a toehold for the free target DNA to hybridize and displace one of the constituent strands of the HJ molecule. Figure 3 demonstrates that the presence of an overhang does not yield an observable interference with the fluctuations. We report on the capture of HJ-10 molecules (HJ with a 10-nucleotide polyA ssDNA overhang), and Figure 3A shows a distribution of all-points histograms from 15 different HJ-10 capture events.

We see Type 1 (red), Type 2 (orange), and Type 3 (teal) distributions similar to those seen for HJ-0, but we also see a new type of event (Type 4, green) that results from rapid, downward-going transitions to a deeper substate. We hypothesize that the Type 4 fluctuations result from the 10 nucleotide overhang inserting into the vestibule region of the

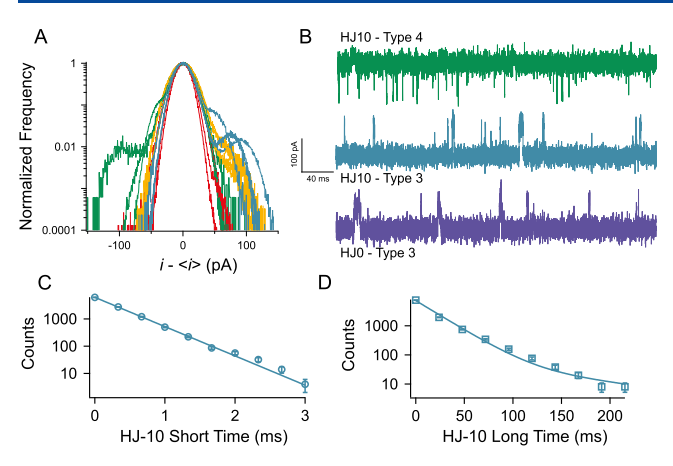


Figure 3. HJ-10 fluctuations showing similar trends as the HJ-0 molecules. (A) Normalized and rescaled current histograms for 15 different HJ-10 capture events. The red and orange histograms correspond to the Type 1 and Type 2 fluctuations from Figure 2. A new fluctuation type (Type 4, green) shows negative-going current fluctuations. (B) Sample current traces illustrate the nature of each fluctuation type. We include HJ-0 Type 3 fluctuations from Figure 2 (blue) to compare with the corresponding HJ-10 Type 3 fluctuations (teal). (C) Short-time and (D) long-time distributions of the Type-3 HJ-10 kinetics are well-fit with single and double exponential functions, respectively (solid lines). Data shown here were collected in 3 M KCl at pH 7.4 under a +140 mV applied transmembrane potential. Residence time distributions were constructed from three different HJ-10 molecules.

pore and interacting across the constriction region into the *trans*-side lumen, which is known to create deep current blockades. Further analysis of a slower and rarer *trans*-side

probing fluctuation, which we refer to as "Type 5", can be found in section 3 of the Supporting Information.

Sample current traces for Type 3 and Type 4 HJ-10 events along with an HJ-0 Type 3 event are shown in Figure 3B. Type 3 events seem very similar between HJ-0 and HJ-10 molecules, as one might expect, given the fact that Type 3 events most likely result from the overhang remaining outside the nanopore region. A kinetic analysis of HJ-10 Type 3 events shows similar short- and long-time distributions as those seen in Figure 2C,D. A more complete discussion of the full current traces associated with the different current blockade types, along with a summary of current blockade frequency distributions across all HJ constructs used throughout the manuscript, can be found in sections 2–4 of the Supporting Information.

Fits to the distributions yield a mean short time of  $t_{\rm short} = (0.40 \pm 0.01)$  ms and a mean long time of  $t_{\rm long,1} = (21 \pm 1)$  ms and  $t_{\rm long,2} = (100 \pm 20)$  ms. This corresponds to kinetic rates of  $k_{\rm fast} = (2500 \pm 100)$  s<sup>-1</sup> and  $k_{\rm slow,1} = (48 \pm 2)$  s<sup>-1</sup>,  $k_{\rm slow,2} = (10 \pm 2)$  s<sup>-1</sup>. This is in close agreement with the HJ-0 kinetic results in Figure 2.

Given that the rapid, Type 3, fluctuations seen in Figures 1–3 result from transitions between different HJ configurations, we propose to utilize nanopore sensing in conjunction with trapped HJ molecules as a short-DNA oligo sensor whereby the introduction of a specific target DNA will modify the two-state Type 3 fluctuations upon hybridization of the target with the fluctuating HJ molecule.

Figure 4A,B shows a schematic illustration of the process where a trapped HJ with an eight-nucleotide overhang on one of its arms (hereafter HJ-8) fluctuates inside the  $\alpha$ HL pore. Target ssDNA (T) with a sequence complementary to one of

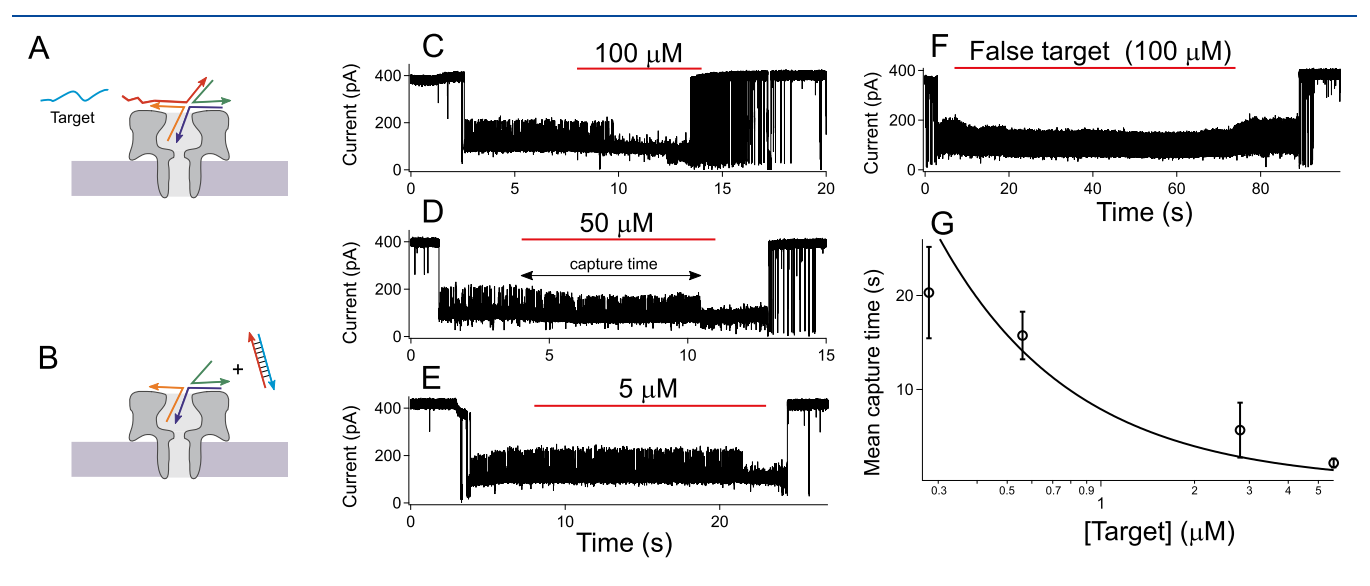


Figure 4. HJ-8 captured and sprayed with various concentrations of target shows clear evidence of binding. (A) Representation of a toehold-mediated HJ-8 electrophoretically captured in a pore, which is then exposed by the target molecules complementary to a toehold strand. (B) Schematic showing strand displacement after toehold strand hybridizes with its complementary target. (C–E) Sample traces show individual capture events followed by spraying of a target DNA strand that can displace the HJ overhang. The red bar in each trace corresponds to the time when the DNA target spray was on. The sudden loss of fluctuations at t  $\approx$  9, 11, and 22 s for (C), (D), and (E), respectively, is evidence of the target binding to the HJ construct. Target concentrations correspond to concentration in the microcapillary tip. (F) Spraying with 100  $\mu$ M false target yields no binding event over an extended period of time. (G) The mean capture time (capture time is defined as the time from the start of the target spray until the HJ-fluctuations cease) calculated from a minimum of three capture events with corresponding standard errors decreases with increasing target concentration as expected. The solid line is a one-parameter weighted fit with  $T_{\text{capture}} = (k_{\text{on}}C)^{-1}$  from which we extract an onrate value of  $k_{\text{on}} = (1.3 \pm 0.1) \times 10^5 \, \text{M}^{-1} \, \text{s}^{-1}$ . Note that the reported target analyte concentrations in (G) are estimated at the pore from current blockade statistics. A more complete discussion of this point can be found in the Supporting Information. All data shown were collected in 3 M KCl at pH 7.4 under an applied transmembrane potential of +140 mV.

the HJ-8 strands is ejected onto the molecule, and hybridization between the target and the extended arm of the HJ-8 leads to the partial or full disassembly of HJ-8, yielding no noticeable fluctuations. Figure 4C shows a sample current trace of the experiment where an HJ-8 molecule is trapped in the pore, and after several seconds a second capillary microtip ejects 100  $\mu$ M of the ssDNA target onto the pore. After a few seconds, the two-state fluctuations stop, indicating that the target hybridized to the HJ-8 molecule and removed the complementary probe strand.

The main idea here is to trap a modified HJ-8 molecule, which exhibits Type 3 fluctuations (two-state) so that the overhang lying outside the channel is free to interact with the external analyte (target strand). As the toehold-mediated strand displacement (TMSD) greatly accelerates the reaction rate 106-fold, 51 the junction should instantly stabilize into a new fluctuation type. Figure 4C-E shows typical current traces of analyte-HJ-8 binding events at different analyte concentrations (100, 50, and 5  $\mu$ M in the ejecting tip). The red bar in each trace corresponds to the time interval during which the DNA target was ejected onto the pore. For the negative control, we performed experiments with a false target (FT) that consisted of a single mismatched nucleotide. Spraying 100 uM of this FT onto the nanopore-bound HJ-8 did not yield any change to the fluctuations over an extended period (see Figure 4F).

Figure 4G shows that the binding reaction rate increases with the target concentration as expected. Assuming first-order reaction rate kinetics, the capture time scales inversely with the analyte concentration as  $T_{\text{capture}} = (k_{\text{on}}C)^{-1}$ , where C is the concentration of the analyte at the pore and not the pipet tip. Diffusion of the target analyte as it leaves the capillary tip will reduce the concentration from the known value in the tip. This requires that we rescale the target concentration from the values reported in the capillary tip (Figure 4C–E) to estimate values at the pore entrance. A thorough discussion of our estimation protocol is detailed in section 5 of the Supporting Information. From the weighted least-squares fit to the capture time data in Figure 4G, we find an on rate of  $k_{\rm on} = (1.3 \pm 0.1)$  $\times$  10<sup>5</sup> M<sup>-1</sup> s<sup>-1</sup>, which is in reasonable agreement with previously reported values for DNA hybridization using toehold.53

To further verify that the binding of target DNA to the overhang portion of the HJ molecule modifies the HJ fluctuations in a manner consistent with the nanopore results, we performed target binding experiments with the more traditional smFRET technique. The sequence used in the FRET experiments is based on an HJ-6 sequence that differs slightly from the HJ-8 molecule used in the nanopore experiments. While we noticed that the binding of the target with 6-nt toehold is not as efficient as with 8-nt toehold in nanopore experiments, perhaps due to unspecified interference from the microenvironment around the nanopore, we decided to use 6-nt toehold in smFRET experiments, as this was proven to work in the FRET setup before. 9,53

A Cy3-Cy5 donor—acceptor pair was incorporated into the construct as shown in Figure 5A. This modification allows one to image the conformational dynamics of the HJ as it switches between the different isomer conformations. <sup>17,49,50</sup> We chose to use 1 M KCl with 50 mM MgCl<sub>2</sub> to make the solvent environment similar to the nanopore experiment in terms of ionic strength and at the same time slow down the HJ fluctuations using divalent cations (Mg<sup>2+</sup>) to make them

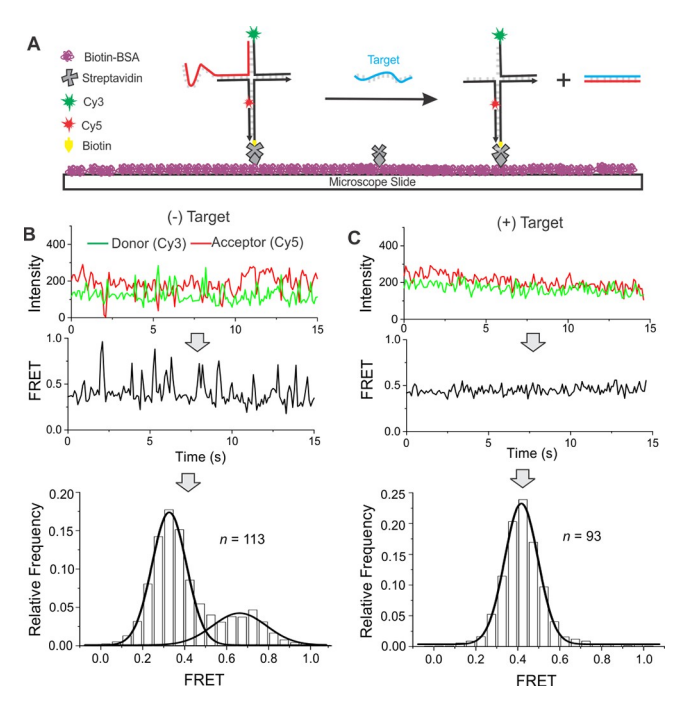


Figure 5. Single-molecule FRET analysis of HJ as a sensor. (A) Experimental setup for the smFRET analysis. The biotin-labeled HJ was surface-immobilized on a biotinylated BSA (bBSA)/streptavidincoated quartz slide. The construct was labeled with a Cy3/Cy5 fluorophore pair to enable FRET. One of the strands forming the junction was extended to create a 6nt sticky end, which serves as a probe. It is designed in a way that, when the sensor is exposed to its target (T6, a DNA strand fully complementary to probe), removal of the probe strand from the junction is expected. (B, C) smFRET data in the absence (-Target) and presence (+Target) of the target. The top panels show typical intensity-time traces. In the absence of the target, there was an anticorrelated switching of the donor/acceptor intensities corresponding to the conformational dynamics inherent to a fully formed HJ. With the addition of the target, these intensity traces were relatively flat, indicating a cessation of HJ dynamics in a target-dependent manner. The middle panels show the calculated FRET efficiency for the typical intensity-time traces, and the bottom panels show corresponding histograms from a large set of molecules. While the fully formed HJ showed a bimodal distribution, there was only one population in the presence of the target. This result showed that, in addition to the nature of FRET traces, the distribution of FRET populations can also be used as a detection signal. The histograms were prepared using the first 200 data points of each FRET trace and binned at 0.05 FRET before being plotted. The curves in the histograms represent one- or two-peak Gaussian fitting to determine mean FRET efficiencies. All smFRET experiments were performed in KCl buffer (1 M KCl, 137 mM NaCl, 50 mM MgCl<sub>2</sub>, 12 mM phosphate) in the presence of an oxygen-scavenging system (OSS, 5 mM trolox, 2 mM protocatechuic acid, 50 nM protocatechuate 3,4-dioxygenase at pH 7.4) to retard photobleaching of the fluorophores.

observable with the smFRET technique. The resulting measurements showed dynamic traces (Figure 5B) with interconvertible switching between low ( $E\approx 0.3$ ) and high ( $E\approx 0.7$ ) FRET states that are consistent with the previous results <sup>17</sup> of the HJ's conformational dynamics under high ionic strength. A histogram of the measured FRET data showed clear evidence of a bimodal distribution representing the two isomeric states of the HJ. Further analysis of these dynamic traces (n=468 transitions) using Hidden Markov's Model (HMM) yielded an average dwell time of 0.609 and 0.150 s for

the low- and high-FRET states corresponding to the transition rates of 1.64 and 6.66 s<sup>-1</sup>, respectively. Although these transition rates are much slower than what is observed in the nanopore results in Figures 2 and 3 (with the exception of  $k_{\rm slow,2}$ ), this is expected due to the use of high Mg<sup>2+</sup> in the smFRET experiments.

Our interest is in exploring the effect that target binding has on the HJ fluctuations and seeing if the observed "freezing out" of the fluctuations seen in the nanopore (Figure 4C–E) also occurs in the smFRET experiments. Figure 5C confirms this behavior where, upon addition of the target strand T6 (400 nM), we observed that the vast majority of traces are nondynamic with the FRET level remaining fixed at  $E\approx 0.4$ . This conversion of a dynamic to a stable FRET state following binding of the target molecule indicates that the target DNA successfully disassembled the four-way junction. This observation supports our assertion that the nanopore is capable of measuring binding kinetics based on how the HJ fluctuation changes in the presence of a target.

#### CONCLUSIONS

Analyzing single-molecule fluctuations provides a critical understanding of the various mechanisms underlying Holliday junction behavior. Given the central role of HJs in HR and dsDNA break repair, it is important to provide as many measurement modalities as possible to better understand their inherent fluctuations. In this work, we explored the use of nanopore sensing with a biological pore ( $\alpha$ HL), which has traditionally focused on single-stranded DNA and RNA given the size constrictions imposed by the pore geometry. Our results show that the conformational fluctuations happening outside the nanopore can lead to clearly observable current fluctuations. The advantage of nanopore sensing is twofold in that they enable label-free detection without the need for artificially immobilizing the molecule to a surface, and they provide high temporal-bandwidth detection ( $B \approx 10 \text{ kHz}$ ), which should enable one to observe rapid conformational fluctuations. To confirm that the observed fluctuations result from the inherent HJ-conformational switching rather than spurious noise, we performed a control experiment with a modified HJ (I-HJ-0) where a mismatched sequence at the core of the junction eliminated conformational fluctuations.

Targeting HJs is crucial for the HR regulation process in repairing DNA damage and maintaining genome integrity. Therefore, HJ modifications represent a highly promising therapeutic target. 9,54,55 With this potential application in mind, we also demonstrated target binding kinetics with specific targets. Both examples demonstrated that the observed fluctuations most likely result from the inherent HJ conformational fluctuations. This is important because the observed fluctuation kinetics are on the order of milliseconds, which are too rapid to be observed with standard single-molecule techniques such as smFRET. The two major results are the increased kinetics associated with HJ fluctuations in a nanopore environment without having to slow down the kinetics using divalent cations and the ability to utilize the pore-bound single HJ molecule as a sensor for detecting target DNA. These results suggest future work to possibly apply simulations to investigate how the nanopore evnironment stabilizes different HJ conformers and also to explore other ligands such as small molecules and HJ-binding peptides and understand their binding kinetics, induced HJ fluctuations, and

the roles they might have in the development of HJ-based therapeutics.

#### ASSOCIATED CONTENT

## Supporting Information

The Supporting Information is available free of charge at https://pubs.acs.org/doi/10.1021/acs.analchem.2c00342.

DNA constructs, sample current traces (HJ-0, HJ-8, and HJ-10), overhang-induced nanopore fluctuations (i.e., Type 5 fluctuations), frequency of blockade types of each HJ construct, accurate estimation of the target onrate (PDF)

#### AUTHOR INFORMATION

#### Corresponding Author

Joseph E. Reiner — Department of Physics, Virginia Commonwealth University, Richmond, Virginia 23284, United States; Email: jereiner@vcu.edu

#### **Authors**

Madhav L. Ghimire – Department of Physics, Virginia Commonwealth University, Richmond, Virginia 23284, United States

Dalton R. Gibbs – Department of Chemistry, Virginia Commonwealth University, Richmond, Virginia 23284, United States

Roaa Mahmoud – Department of Chemistry, Virginia Commonwealth University, Richmond, Virginia 23284, United States

Soma Dhakal – Department of Chemistry, Virginia Commonwealth University, Richmond, Virginia 23284, United States

Complete contact information is available at: https://pubs.acs.org/10.1021/acs.analchem.2c00342

# **Author Contributions**

The manuscript was written through contributions of all authors. All authors have given approval to the final version of the manuscript.

### Notes

The authors declare no competing financial interest.

# ACKNOWLEDGMENTS

J.E.R. acknowledges funding from the National Science Foundation under Grant No. CBET-2011173. Additional funding was provided by the Virginia Commonwealth University-CHS SEED fund for S.D. and J.E.R. FRET experiments were supported by the VCU Startup fund for S.D.

#### REFERENCES

- (1) Lieber, M. R. Annu. Rev. Biochem. 2010, 79 (1), 181-211.
- (2) Holliday, R. Genet. Res. 1964, 5 (2), 282-304.
- (3) Potter, H.; Dressler, D. Proc. Natl. Acad. Sci. U.S.A. 1976, 73 (9), 3000–3004
- (4) Schwacha, A.; Kleckner, N. Cell 1995, 83, 783-791.
- (5) Sobell, H. M. Proc. Natl. Acad. Sci. U.S.A. 1972, 69 (9), 2483–2487.
- (6) Brogden, A. L. The Holliday Junction as a Therapeutic Target: Synthetic and Structural Studies of the Interactions of Small Molecules with Nucleic Acid Structures, PhD Thesis, University College London: England, 2006.

- (7) Kato, T.; Sato, N.; Hayama, S.; Yamabuki, T.; Ito, T.; Miyamoto, M.; Kondo, S.; Nakamura, Y.; Daigo, Y. *Cancer Res.* **2007**, *67* (18), 8544–8553.
- (8) Yao, F.; An, Y.; Li, X.; Li, Z.; Duan, J.; Yang, X.-D. Int. J. Nanomedicine 2020, 15, 2119–2129.
- (9) Megalathan, A.; Wijesinghe, K. M.; Dhakal, S. ACS Sens. 2021, 6 (3), 1367–1374.
- (10) Goyal, N.; Rossi, M. J.; Mazina, O. M.; Chi, Y.; Moritz, R. L.; Clurman, B. E.; Mazin, A. V. Nat. Commun. 2018, 9 (1), 34.
- (11) Papadakis, G.; Tsortos, A.; Gizeli, E. Nano Lett. 2010, 10, 5093-5097.
- (12) Gibbs, D. R.; Mahmoud, R.; Kaur, A.; Dhakal, S. *Biophys. J.* **2021**, 120 (10), 1894–1902.
- (13) Gibbs, D. R.; Dhakal, S. Int. J. Mol. Sci. 2019, 20 (23), 6102.
- (14) Hohng, S.; Zhou, R.; Nahas, M. K.; Yu, J.; Schulten, K.; Lilley, D. M. J.; Ha, T. Science **2007**, 318 (5848), 279–283.
- (15) Yu, J.; Ha, T.; Schulten, K. Nucleic Acids Res. 2004, 32 (22), 6683-6695.
- (16) Roy, R.; Hohng, S.; Ha, T. Nat. Methods 2008, 5 (6), 507–516.
- (17) Gibbs, D. R.; Dhakal, S. Biochemistry 2018, 57 (26), 3616–3624.
- (18) Sauer-Budge, A. F.; Nyamwanda, J. A.; Lubensky, D. K.; Branton, D. *Phys. Rev. Lett.* **2003**, *90* (23), 238101.
- (19) Akeson, M.; Branton, D.; Kasianowicz, J. J.; Brandin, E.; Deamer, D. W. *Biophys. J.* **1999**, 77 (6), 3227–3233.
- (20) Kasianowicz, J. J.; Brandin, E.; Branton, D.; Deamer, D. W. *Proc. Natl. Acad. Sci. U.S.A.* **1996**, 93 (24), 13770–13773.
- (21) Megalathan, A.; Cox, B. D.; Wilkerson, P. D.; Kaur, A.; Sapkota, K.; Reiner, J. E.; Dhakal, S. *Nucleic Acids Res.* **2019**, *47* (14), 7199–7212
- (22) Shim, J. W.; Gu, L.-Q. J. Phys. Chem. B 2008, 112 (28), 8354–8360
- (23) Vercoutere, W.; Winters-Hilt, S.; Olsen, H.; Deamer, D.; Haussler, D.; Akeson, M. Nat. Biotechnol. 2001, 19 (3), 248-252.
- (24) Ussery, D. W.; Sinden, R. R. Biochemistry 1993, 32 (24), 6206–6213.
- (25) Ayub, M.; Bayley, H. Nano Lett. 2012, 12 (11), 5637-5643.
- (26) Purnell, R. F.; Schmidt, J. J. ACS Nano 2009, 3 (9), 2533–2538.
- (27) Howorka, S.; Cheley, S.; Bayley, H. Nat. Biotechnol. 2001, 19 (7), 636-639.
- (28) Kasianowicz, J. J.; Robertson, J. W. F.; Chan, E. R.; Reiner, J. E.; Stanford, V. M. *Annu. Rev. Anal Chem.* **2008**, *1* (1), 737–766.
- (29) Reiner, J. E.; Balijepalli, A.; Robertson, J. W. F.; Campbell, J.; Suehle, J.; Kasianowicz, J. J. *Chem. Rev.* **2012**, *112* (12), 6431–6451.
- (30) Robertson, J. W. F.; Ghimire, M. L.; Reiner, J. E. Biochimica et Biophysica Acta (BBA) Biomembranes 2021, 1863 (9), 183644.
- (31) Zhang, X.; Price, N. E.; Fang, X.; Yang, Z.; Gu, L.-Q.; Gates, K. S. ACS Nano 2015, 9 (12), 11812–11819.
- (32) Wloka, C.; Mutter, N. L.; Soskine, M.; Maglia, G. Angew. Chem., Int. Ed. 2016, 55 (40), 12494–12498.
- (33) Dekker, C. Solid-State Nanopores. In *Nanoscience and Technology;* Co-Published with Macmillan Publishers Ltd: UK, 2009; pp 60–66.
- (34) Pham, B.; Eron, S. J.; Hill, M. E.; Li, X.; Fahie, M. A.; Hardy, J. A.; Chen, M. *Biophys. J.* **2019**, *117* (5), 844–855.
- (35) Rotem, D.; Jayasinghe, L.; Salichou, M.; Bayley, H. J. Am. Chem. Soc. 2012, 134 (5), 2781–2787.
- (36) Rosenstein, J.; Sorgenfrei, S.; Shepard, K. L. 2011 IEEE Cust. Integr. Circuits Confer. (CICC) 2011, 1-7.
- (37) Chernikova, S. B.; Game, J. C.; Brown, J. M. Cancer Biol. Ther. **2012**, 13 (2), 61–68.
- (38) Helleday, T.; Petermann, E.; Lundin, C.; Hodgson, B.; Sharma, R. A. *Nat. Rev. Cancer* **2008**, *8* (3), 193–204.
- (39) Miyagawa, K. Cancer Sci. 2008, 99 (2), 187–194.
- (40) Moynahan, M. E.; Jasin, M. Nat. Rev. Mol. Cell Biol. 2010, 11 (3), 196–207.
- (41) Kaur, A.; Sapkota, K.; Dhakal, S. ACS Sens. 2019, 4 (3), 623-633.

- (42) Aitken, C. E.; Marshall, R. A.; Puglisi, J. D. *Biophys. J.* **2008**, 94 (5), 1826–1835.
- (43) Angevine, C. E.; Robertson, J. W. F.; Dass, A.; Reiner, J. E. Laser-Based Temperature Control to Study the Roles of Entropy and Enthalpy in Polymer-Nanopore Interactions. *Sci. Adv.* **2021**, *7* (17), eabf5462.
- (44) Chavis, A. E.; Brady, K. T.; Hatmaker, G. A.; Angevine, C. E.; Kothalawala, N.; Dass, A.; Robertson, J. W. F.; Reiner, J. E. ACS Sens. **2017**, 2 (9), 1319–1328.
- (45) Cox, B. D.; Ghimire, M. L.; Bertino, M. F.; Reiner, J. E. ACS Appl. Nano Mater. **2020**, 3 (8), 7973–7981.
- (46) Menestrina, G. J. Membr. Biol. 1986, 90 (2), 177-190.
- (47) Gibbs, D. R.; Kaur, A.; Megalathan, A.; Sapkota, K.; Dhakal, S. *Methods Protoc.* **2018**, *1* (4), 40.
- (48) Tokunaga, M.; Kitamura, K.; Saito, K.; Iwane, A. H.; Yanagida, T. *Biochem. Biophys. Res. Commun.* **1997**, 235 (1), 47–53.
- (49) Hyeon, C.; Lee, J.; Yoon, J.; Hohng, S.; Thirumalai, D. Nat. Chem. 2012, 4 (11), 907–914.
- (50) Joo, C.; McKinney, S. A.; Lilley, D. M. J.; Ha, T. *J. Mol. Biol.* **2004**, 341 (3), 739–751.
- (51) Yurke, B.; Turberfield, A. J.; Mills, A. P.; Simmel, F. C.; Neumann, J. L. *Nature* **2000**, 406 (6796), 605–608.
- (52) Zhang, D. Y.; Winfree, E. J. Am. Chem. Soc. 2009, 131 (47), 17303-17314.
- (53) Sapkota, K.; Kaur, A.; Megalathan, A.; Donkoh-Moore, C.; Dhakal, S. Sensors **2019**, *19* (16), 3495.
- (54) Li, T.; Yao, F.; An, Y.; Li, X.; Duan, J.; Yang, X.-D. Molecules **2021**, 26 (4), 1067.
- (55) Sarkar, S. K.; Andoy, N. M.; Benítez, J. J.; Chen, P. R.; Kong, J. S.; He, C.; Chen, P. *J. Am. Chem. Soc.* **2007**, 129 (41), 12461–12467.

# **□** Recommended by ACS

#### Single-Molecule Force Spectroscopy of Deoxyribonucleic Acid and Deoxyribonucleic Acid Polymerase Activity Impacted by Alkylating Agents

Tianyu Cai, Huizhong Xu, et al.

MAY 17, 2023

THE JOURNAL OF PHYSICAL CHEMISTRY LETTERS

READ 🗹

### Analysis of Megadalton-Sized DNA by Charge Detection Mass Spectrometry: Entropic Trapping and Shearing in Nanoelectrospray

Lohra M. Miller, Martin F. Jarrold, et al.

JUNE 02, 2023

ANALYTICAL CHEMISTRY

READ 🗹

# Metabolic Footprinting-Based DNA-AuNP Encoders for Extracellular Metabolic Response Profiling

Guangpei Qi, Xiangmeng Qu, et al.

MAY 08, 2023

ANALYTICAL CHEMISTRY

READ 🗹

### Force-Dependent Intercalative Bulky DNA Adduct Formation Detected by Single-Molecule Stretching

Yajun Liu, Huijuan You, et al.

SEPTEMBER 21, 2022

ANALYTICAL CHEMISTRY

READ 🗹

Get More Suggestions >